*Meteoritics & Planetary Science* 37, 1781–1796 (2002)
Available online at http://www.uark.edu/meteor

# Mineralogy and petrology of amoeboid olivine inclusions in CO3 chondrites: Relationship to parent-body aqueous alteration

LYSA J. CHIZMADIA[1†*], ALAN E. RUBIN[2] AND JOHN T. WASSON[1,2,3]

[1]Department of Earth and Space Sciences, University of California, Los Angeles, California 90095-1567, USA
[2]Institute of Geophysics and Planetary Physics, University of California, Los Angeles, California 90095-1567, USA
[3]Department of Chemistry and Biochemistry, University of California, Los Angeles, California 90095, USA
†Present address: Department of Earth and Planetary Sciences, University of New Mexico, Albuquerque, New Mexico 87131, USA
*Correspondence author's e-mail address: lchiz@unm.edu

*(Received 2001 June 6; accepted in revised form 2002 August 20)*

**Abstract**–Petrographic and mineralogic studies of amoeboid olivine inclusions (AOIs) in CO3 carbonaceous chondrites reveal that they are sensitive indicators of parent-body aqueous and thermal alteration. As the petrologic subtype increases from 3.0 to 3.8, forsteritic olivine ($Fa_{0-1}$) is systematically converted into ferroan olivine ($Fa_{60-75}$). We infer that the Fe, Si and O entered the assemblage along grain boundaries, forming ferroan olivine that filled fractures and voids. As temperatures increased, $Fe^{+2}$ from the new olivine exchanged with $Mg^{+2}$ from the original AOI to form diffusive haloes around low-FeO cores. Cations of $Mn^{+2}$, $Ca^{+2}$ and $Cr^{+3}$ were also mobilized.

The systematic changes in AOI textures and olivine compositional distributions can be used to refine the classification of CO3 chondrites into subtypes. In subtype 3.0, olivine occurs as small forsterite grains ($Fa_{0-1}$), free of ferroan olivine. In petrologic subtype 3.2, narrow veins of FeO-rich olivine have formed at forsterite grain boundaries. With increasing alteration, these veins thicken to form zones of ferroan olivine at the outside AOI margin and within the AOI interior. By subtype 3.7, there is a fairly broad olivine compositional distribution in the range $Fa_{63-70}$, and by subtype 3.8, no forsterite remains and the high-Fa peak has narrowed, $Fa_{64-67}$. Even at this stage, there is incomplete equilibration in the chondrite as a whole (*e.g.*, data for coarse olivine grains in Isna (CO3.8) chondrules and lithic clasts show a peak at $Fa_{39}$). We infer that the mineral changes in AOI identified in the low petrologic types required aqueous or hydrothermal fluids whereas those in subtypes ≥3.3 largely reflect diffusive exchange within and between mineral grains without the aid of fluids.

## INTRODUCTION

McSween (1977a) was the first to organize the CO3 chondrites into a metamorphic sequence. He defined stages I–III on the basis of the degree of textural recrystallization, decreasing heterogeneity in mafic mineral compositions and increasing FeO enrichment in the mafic minerals. With increasing metamorphism, the amount of chondrule glass and the abundances of metallic grains, presolar diamonds, bulk volatiles and noble gases decrease (McSween, 1977a,b; Huss, 1990). Scott and Jones (1990) refined the metamorphic series and defined subtypes 3.0–3.7 on the basis of igneous zoning in chondrule phenocrysts and increasing FeO concentration at the edges and cracks of these phenocrysts. Keck and Sears (1987) used peak thermoluminescence (TL) temperatures to classify the CO3 chondrites into subtypes that differed slightly from those of Scott and Jones.

Several authors have attributed some of the alteration of CO3 chondrites to hydrothermal processes. For example, Kerridge (1972) suggested that iron mobilization in chondrule olivine phenocrysts along cracks was due to fluid alteration. Kojima *et al.* (1995) ascribed similar iron enrichment in amoeboid olivine inclusions (AOIs) of Antarctic CO3 chondrites to aqueous processes.

Rubin (1998) noted that several systematic changes of CO3 chondrite properties with increasing petrologic subtype could be interpreted as evidence of fluid alteration. These include the erosion of chondrule surfaces, the formation of phyllosilicates and hydrous ferric oxides (Ikeda, 1983; Keller and Buseck, 1990; Brearley, 1993), an increase in the apparent percentage of "rimmed" AOIs, a decrease in the abundance of small chondrules, and an increase in the whole-rock $\Delta^{17}O$ ($=\delta^{17}O - 0.52 \times \delta^{18}O$) values, an apparent indication of increasing degree of alteration by water having higher $\Delta^{17}O$ (Clayton, 1993; Clayton and Mayeda, 1999; Clayton *et al.*, 1976; Hiyagon and Hashimoto, 1999).

Amoeboid olivine inclusions in CO3 chondrites are irregularly shaped, fine-grained objects that constitute a few



Prelude preprint MS#4566

volume-percent of individual meteorites in most carbonaceous chondrite groups. They consist of major olivine and minor amounts of moderately refractory minerals such as anorthitic plagioclase, aluminum- and titanium-bearing diopside, and in some cases, spinel ($MgAl_2O_4$) (Fig. 1). Low-Ca pyroxene is absent in all subtypes.

It is important to note that there are different names for what we call AOIs. Some researchers call them amoeboid olivine aggregates (AOA), but AOIs are relatively compact objects whereas the term "aggregate" implies high-intergranular porosity. Interlocking grains are common in AOIs in CO3.0 chondrites. We, therefore, prefer the more neutral, less model-dependent term, AOIs.

Most past AOI studies were of inclusions in the Allende CV3 chondrite (*e.g.*, Grossman and Steele, 1976; Hashimoto and Grossman, 1987). Kornacki and Wood (1984) defined two types of AOIs in Allende, "rimmed" and "unrimmed", based on the presence or absence of coarse ferroan olivine near the AOI margin. Broad-beam electron probe analyses of AOIs in CO3 chondrites by McSween (1977b) showed that the FeO, MgO and MnO contents vary with whole-rock metamorphic subtype. In a study of AOIs in reduced CV3 chondrites, Komatsu *et al.* (2001) found a ferroan enrichment pattern similar to the one we report below, which they attributed to secondary thermal metamorphism. They also ascribed the anorthite–diopside–spinel assemblages in the AOI to incorporated refractory inclusions.

The AOIs in CO3 chondrites are similar to those in CV3 chondrites in terms of mineralogy, abundance, shape and texture. However, the AOIs in CO3 chondrites are much

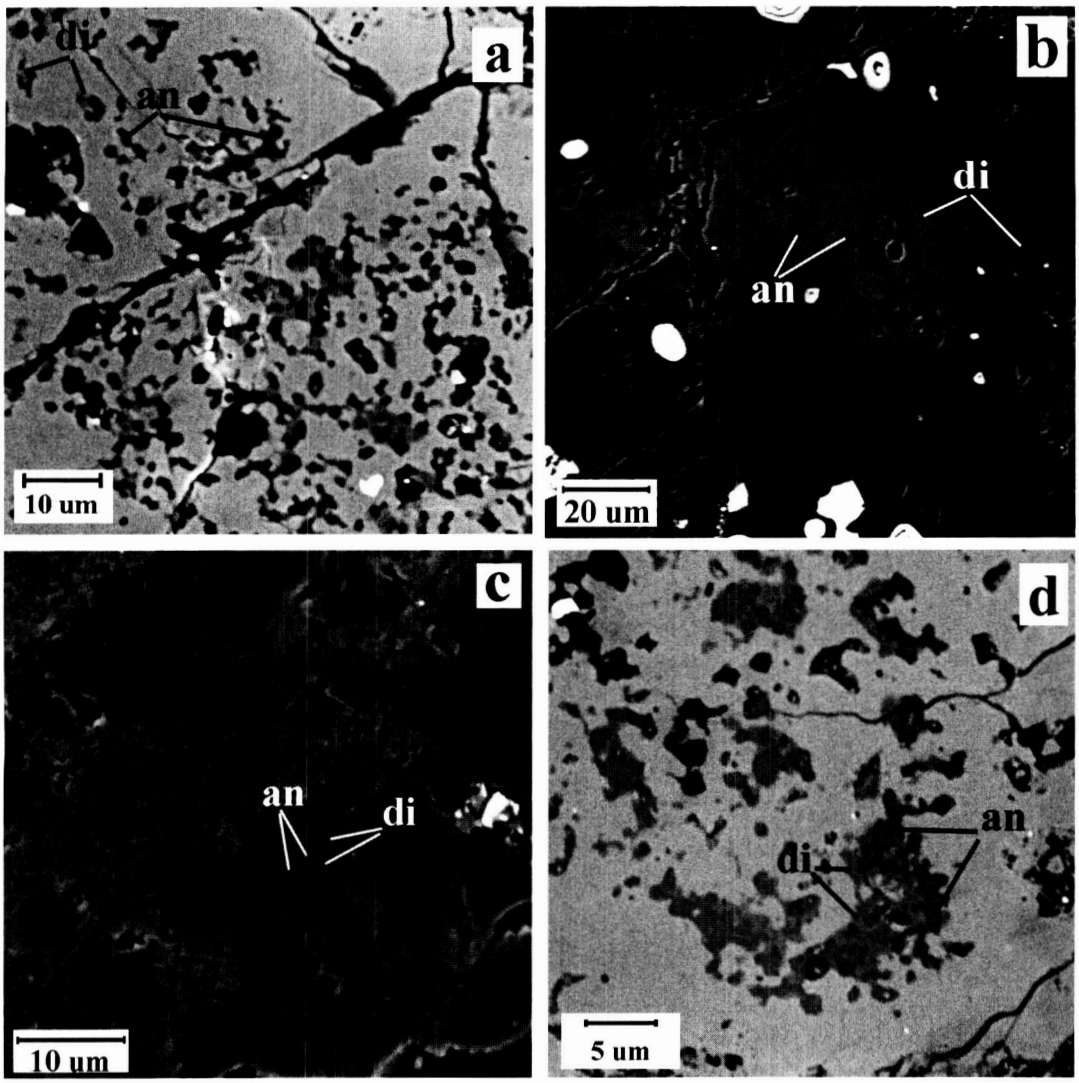


FIG. 1. Backscattered electron images of the relationships between anorthite and diopside in CO3 amoeboid olivine inclusions. In every case, these phases are surrounded by olivine. (a) Isolated grains of diopside and anorthite in CO3.7 Warrenton. (b) Diopside (light gray) rimming anorthite (medium gray) in CO3.0 ALHA77307. (c) Intergrown diopside (medium gray) and anorthite (dark gray) in CO3.2 Y-82050. (d) Intergrown diopside (medium gray) and anorthite (dark gray) in CO3.8 Isna.

smaller and have smaller grain sizes than their counterparts in CV3 chondrites.

To document the role of alteration, we investigated AOIs in 12 CO3 chondrites that span the range of petrologic subtypes. CO3 AOIs are fine-grained and thus have high surface-area/volume ratios and small lattice-diffusion path lengths. These characteristics lead to the expectation that AOIs should be affected in the early stages of metamorphic or aqueous-alteration processes (McSween, 1977a) and should be sensitive indicators of such alteration. AOIs are present throughout the CO3 metamorphic sequence, and it should be possible to use their textural and mineralogical characteristics to quantify CO3 alteration.

## ANALYTICAL METHODS

Polished thin sections of 12 CO3 chondrites (Table 1) were studied microscopically in transmitted and reflected light. Five AOIs in each meteorite were analyzed for 10 elements with the Cameca "Camebax-microbeam" electron microprobe at UCLA using crystal spectrometers, natural mineral standards, 20 s counting times, PAP corrections (the Cameca version of ZAF corrections), a sample current of ~11 nA and an acceleration voltage of 15 kV. Backscattered electron (BSE) images were made of each AOI at a range of magnifications with the LEO 1430VP scanning electron microscope (SEM) at UCLA using a 15 kV acceleration voltage and a working distance ranging from 17 to 20 mm.

The BSE images were used to determine the modal abundances of low-FeO olivine, ferroan olivine, anorthitic plagioclase, diopsidic pyroxene, spinel, voids and opaque minerals. A 1 × 1 cm acetate grid was laid over the images and the phase (or void) at each intersection was tabulated. Holes clearly due to plucking were excluded, but holes of ambiguous origin that have rounded outlines were counted as voids. The sizes of the inclusions, constituent phases and voids were measured on the BSE images.

TABLE 1. CO3 chondrites and section numbers.

| Meteorite | Subtype | Thin section |
|---|---|---|
| Yamato-81020 | 3.0 | NIPR 56-4 |
| Allan Hills A77307 | 3.0 | ALHA77307,88 |
| Colony | 3.0 | USNM 6264-3 |
| Kainsaz | 3.2 | USNM 2486-8 |
| Rainbow | 3.2 | LC 998 |
| Yamato-82050 | 3.2 | NIPR 101-1 |
| Felix | 3.3 | USNM 235-1 |
| Ornans | 3.4 | USNM 1105-7 |
| Lancé | 3.5 | USNM 380-1 |
| Allan Hills A77003 | 3.6 | ALHA77003,115 |
| Warrenton | 3.7 | USNM 43 |
| Isna | 3.8 | USNM 5890-1 |

Abbreviations: NIPR = National Institute of Polar Research, Japan; USNM = National Museum of Natural History, Smithsonian Institution; LC = UCLA Leonard Collection; ALHA sections from NASA Johnson Space Center.

## RESULTS

### Mineralogy and Petrology of Amoeboid Olivine Inclusions

AOIs constitute 7–16 vol% of the CO3 chondrites (Table 4 of McSween, 1977a) and range in size from ~20 $\mu$m to ~1 mm. The petrographic and mineralogic characteristics of AOIs change with petrologic subtype. In all CO3 subtypes AOIs are fine-grained and have irregular shapes, but these properties change systematically with subtype. AOIs in CO3.0 chondrites tend to have somewhat angular outlines; some are moderately equant (Fig. 2). AOIs in subtypes ≥3.4 tend to have scalloped (amoeboid) morphologies (Fig. 2). Some AOIs have embayments at their surfaces that enhance their irregular morphologies. In CO3.4–3.8 chondrites, chondrules and refractory inclusions that are in the same size range as AOIs exhibit fewer irregular surface features and do not have amoeboid outlines. It is difficult to measure the sizes of AOI silicate grains because most grains are appreciably smaller than the ~30 $\mu$m thickness of the thin sections. Nevertheless, based on BSE images of ferroan olivine outlines in AOIs from CO3.3–3.5 chondrites and olivine crystal surfaces seen in voids, we estimate individual CO3 AOI olivines to range in size from ~2 to 10 $\mu$m.

In CO3.0 chondrites, the best-documented AOIs (Table 2) are about 100–500 $\mu$m in mean diameter. AOIs in Yamato (Y)-81020 (the least-equilibrated CO3 chondrite) contain about 8–20 vol% voids that range from about 0.5 to 60 $\mu$m in size. As discussed above, it is probable that some of the voids resulted from plucking during thin-section preparation. Voids tend to be rounded with olivine crystal edges protruding into them. No glass was observed in AOIs in CO3.0 chondrites or in those of higher petrologic subtype.

On a void-free basis, AOIs in CO3.0 chondrites contain 63.6 ± 8.5 vol% olivine, 16.7 ± 6.4 vol% anorthitic plagioclase, 12.0 ± 4.5 vol% Al- and Ti-bearing diopsidic pyroxene, and 7.7 ± 5.0 vol% opaque phases having a range from 1.7 to 13.9 vol% and a peak at 2–4 vol% (Table 2). A minor fraction of the AOIs also contain spinel. Opaque grains in CO3.0 AOIs are composed of metallic Fe-Ni (mainly kamacite); troilite is rare to absent. The metal grains range in diameter from <1 to ~8 $\mu$m.

The outermost regions of the CO3.0 AOIs are composed of olivine; olivine also commonly surrounds anorthite-diopside patches in the AOI interior. Olivine in CO3.0 AOIs is forsteritic, $Fa_{0-3}$. Because of some enhancement of measured FeO values due to oxides produced during terrestrial weathering, we suggest that the initial (*i.e.*, nebular) range in mole percent Fa was narrower (*i.e.*, $Fa_{0-1}$).

Anorthite and diopside are ubiquitous in AOIs from all CO3 subtypes. These phases tend to form irregular and interlocking

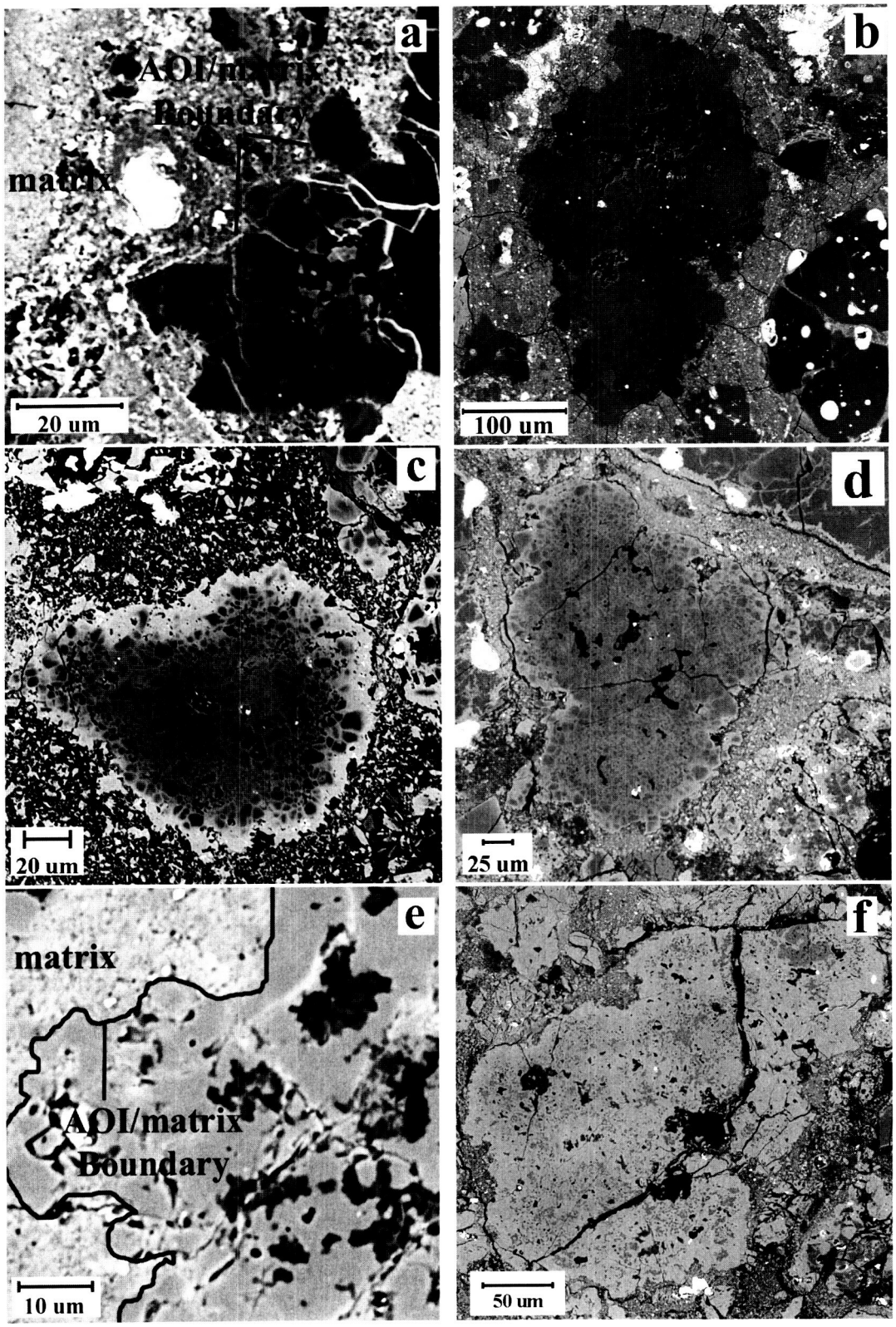


FIG. 2. Backscattered electron images of the irregular surfaces of amoeboid olivine inclusions. (a) AOI from CO3.0 Colony. The AOI is much darker gray than the adjacent portion of the matrix. (b) AOI from CO3.0 ALHA77307. (c) AOI from CO3.4 Ornans. (d) AOI from CO3.3 Felix. (e) AOI from CO3.6 ALHA77003. The inclusion–matrix boundary is outlined in black. (f) AOI from CO3.7 Warrenton. In CO3.0 chondrites, the edges of AOIs appear to reflect fragmentation as opposed to the rounded "amoeboid" shapes present in CO chondrites that experienced more alteration.

TABLE 2. Sizes of selected AOIs and modal abundances of their constituent phases.

| Meteorite | AOI # | Size ($\mu$m) | Olivine (vol%) | Anorthite (vol%) | Diopside (vol%) | Voids (vol%) | Opaques (vol%) |
|---|---|---|---|---|---|---|---|
| Yamato-81020 | 1 | 106 × 153 | 50.4 | 22.7 | 15.1 | 8.4 | 3.4 |
| | 2 | 413 × 538 | 53.1 | 6.2 | 6.2 | 21.9 | 12.5 |
| | 4 | 155 × 329 | 47.7 | 17.4 | 11.9 | 12.8 | 10.1 |
| | 5 | 364 × 536 | 56.8 | 9.5 | 8.4 | 20.0 | 5.3 |
| | 7 | 171 × 400 | 48.6 | 17.1 | 10.5 | 20.0 | 3.8 |
| Allan Hills A77307 | 1 | 211 × 389 | 32.9 | 14.1 | 11.8 | 36.5 | 4.7 |
| | 2 | 188 × 270 | 45.3 | 12.8 | 9.4 | 30.8 | 1.7 |
| | 3 | 156 × 236 | 45.9 | 18.8 | 13.5 | 19.5 | 2.3 |
| | 4 | 413 × 638 | 52.3 | 19.8 | 15.1 | 5.8 | 7.0 |
| | 5 | 103 × 215 | 54.0 | 16.0 | 10.0 | 18.0 | 2.0 |
| Colony | 1 | 132 × 203 | 50.6 | 6.2 | 4.9 | 34.6 | 3.7 |
| | 2 | 68 × 144 | 53.3 | 8.2 | 4.1 | 20.5 | 13.9 |
| | 4 | 74 × 122 | 64.5 | 6.0 | 4.1 | 16.2 | 9.2 |
| Ornans* | 6 | 306 × 375 | 72.8 | 2.6 | 6.1 | 13.2 | 3.5 |
| Lancé* | 13 | 39 × 173 | 56.3 | 16.9 | 4.2 | 15.5 | 4.2 |
| Warrenton | 1 | 529 × 757 | 47.1 | 17.3 | 11.5 | 23.1 | 1.0 |
| | 2 | 250 × 488 | 41.1 | 24.0 | 20.0 | 14.0 | 0.9 |
| | 4 | 289 × 529 | 44.7 | 16.7 | 17.5 | 20.2 | 0.9 |
| | 5 | 282 × 306 | 58.1 | 18.8 | 12.8 | 10.3 | 0.0 |
| | 6 | 524 × 1029 | 64.0 | 12.0 | 8.8 | 15.2 | 0.0 |
| Isna | 1 | 137 × 457 | 47.1 | 14.3 | 10.9 | 27.7 | 0.0 |
| | 3 | 240 × 287 | 55.3 | 11.7 | 7.8 | 25.2 | 0.0 |
| | 4 | 122 × 141 | 68.5 | 14.4 | 7.2 | 9.9 | 0.0 |
| | 5 | 206 × 382 | 65.6 | 16.4 | 11.5 | 4.9 | 1.6 |
| | 6 | 179 × 385 | 49.5 | 22.0 | 17.6 | 8.7 | 2.2 |

*Ornans-6 and Lancé-13 also contain 1.8 and 2.8 vol% spinel, respectively.

grain assemblages ranging from ~5 to 60 $\mu$m (Fig. 1). In some assemblages, diopside rims anorthite; in others, the phases are intergrown. Backscattered electron images show that individual grains of anorthite and diopside in AOIs are rounded and range in diameter from <1 to ~3 $\mu$m in the least (3.0) and most altered (3.7–3.8) subtypes (*i.e.*, there does not appear to be a systematic increase in diopside and anorthite grain size with increasing subtype). From the BSE images it appears that each of the assemblages of anorthite and diopside are composed of numerous smaller crystallites.

On a void-free basis, the best-documented AOIs in CO3.3–3.8 chondrites contain 66.5 ± 10.6 vol% olivine, 18.6 ± 6.2 vol% anorthitic plagioclase, 13.5 ± 5.8 vol% Al- and Ti-bearing diopsidic pyroxene, and 1.4 ± 1.7 vol% opaque phases (Table 2). Spinel ($MgAl_2O_4$), pleonaste ($(Fe,Mg)Al_2O_4$), and a Ca-P phase (probably merrillite) also occur in some of the AOIs. The principal difference in modal mineralogy between AOIs in CO3 chondrites of different subtypes is in the abundance of opaque phases which are particularly low in subtype 3.7–3.8.

The texture of the anorthite-diopside intergrowths changes with increasing subtype (Fig. 1). In the least altered AOIs the anorthite is completely enclosed within the diopside (Fig. 1b). In moderately altered AOIs (Fig. 1c), diopside contains roughly linear patches of anorthite. In the most altered AOIs (Fig. 1a,d), there are discrete grains of diopside and anorthite.

In the most altered CO3 chondrite (subtype 3.8, Isna), all of the AOI olivine is FeO-rich ($Fa_{64-67}$); in chondrites that have experienced intermediate degrees of alteration (*e.g.*, Felix, Ornans, Lancé), the olivine compositional distributions are bimodal (*e.g.*, $Fa_{3-16}$; $Fa_{62-70}$).

Diagrams of minor elements in olivine (*i.e.*, wt% MnO, wt% CaO, wt% $Cr_2O_3$ *vs.* mol% Fa; Fig. 3) show that the MnO, CaO and $Cr_2O_3$ contents in AOI olivine in CO3 chondrites of low petrologic subtype are quite variable whereas those in AOI olivine of high petrologic subtype are much more uniform.

AOIs typically contain several volume-percent opaque minerals. The observed phases include blebs of kamacite, taenite and troilite. Troilite is rare to absent in AOIs from CO3 chondrites of subtype 3.0 and is appreciably more common in AOIs from more-altered CO3 chondrites (subtype 3.4–3.8). Metallic Fe-Ni grains occur in AOIs from all petrologic subtypes. Opaque grains typically range in diameter from <1 to ~10 $\mu$m, although a few rare grains in AOIs from the higher subtypes range up to ~25 $\mu$m. These large opaque grains are almost exclusively troilite.

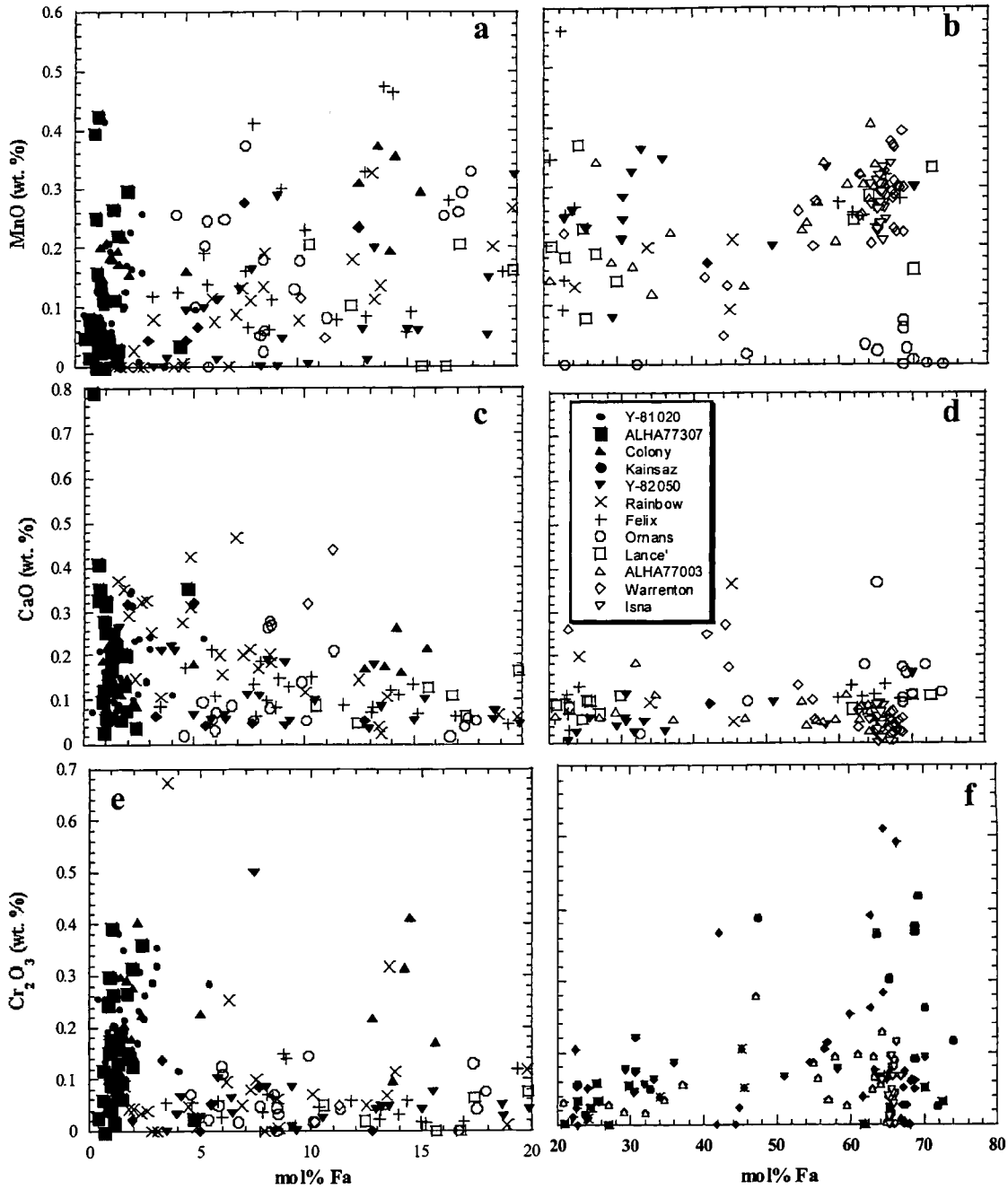


FIG. 3. Minor element concentrations (wt%) *vs.* mol% Fa in AOI olivine grains. All plotted points are from different olivine grains. Individual meteorites are plotted with distinct symbols. (a,b) MnO *vs.* Fa in low-FeO and high-FeO olivines, respectively. (c,d) CaO *vs.* Fa in low-FeO and high-FeO olivines, respectively. (e,f) $Cr_2O_3$ *vs.* Fa in low-FeO and high-FeO olivines, respectively. With increasing petrologic subtype, corresponding to increasing degrees of alteration/metamorphism, the variability in minor element concentrations decreases as equilibrium is approached.

## Spinel-Bearing Amoeboid Olivine Inclusions

Several AOIs containing spinel have been identified in Y-81020, Y-82050, Felix, Ornans, Lancé, Allan Hills (ALH)A77003 and Warrenton. Two spinel-bearing AOIs (one each from Ornans and Lancé) are illustrative of the phase relationships (Fig. 4).

The Ornans AOI is an irregularly shaped 306 × 375 $\mu$m object that contains many cracks and voids (Fig. 4a). The left side of the inclusion is completely normal; it consists of olivine, diopside and anorthite with typical textural relationships. The amount of alteration in this AOI is the same as that found in other AOIs in Ornans. Low-FeO olivine grains are adjacent to ~0.7 to 1.3 $\mu$m thick veins of ferroan olivine (see below). At

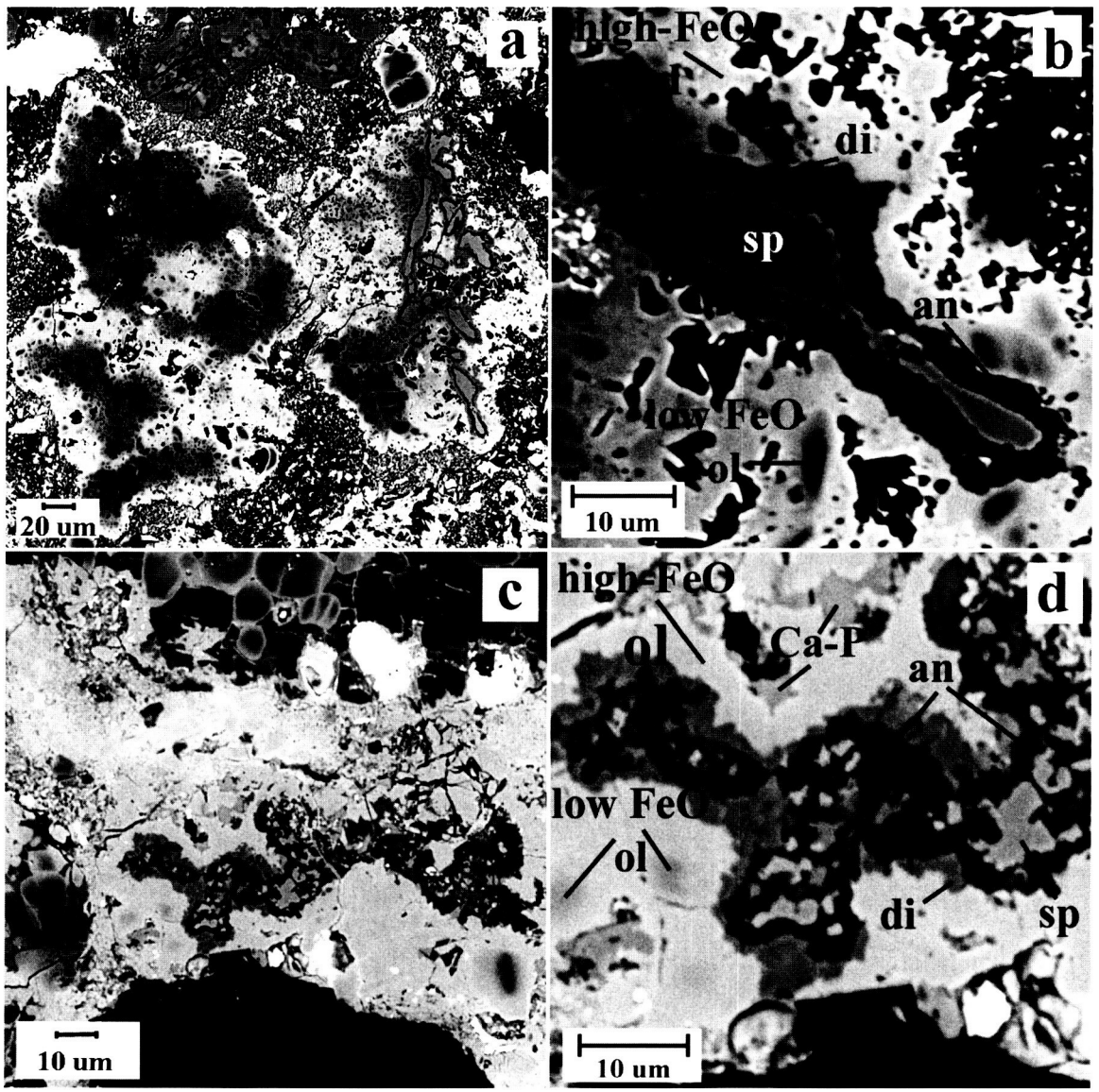


FIG. 4. Backscattered electron images of spinel-rich AOI Ornans-6 and Lancé-13. (a) The entire AOI from CO3.4 Ornans. Elongated spinel laths (light gray) occur within the right side of this inclusion. (b) Enlargement of one of the spinel laths. The spinel grain (medium gray) is surrounded by anorthite (black) that is itself surrounded by diopside (dark gray), indicative of the crystallization sequence. (c) The entire AOI from CO3.5 Lancé. The spinel-rich patches occur in the center of this inclusion. (d) Enlargement of one of the spinel-rich patches. The spinel (light gray) is surrounded by anorthite (dark gray) that is itself surrounded by diopside (medium gray). The degree of olivine alteration in these AOIs is similar to those of non-spinel-bearing AOIs in these same meteorites.

least 12 spinel grains (constituting 2 vol% of the whole AOI) are located on the right side of the inclusion. Most spinel grains are elongated (Fig. 4b), ranging in maximum dimension from ~5 to 47 $\mu$m, appreciably larger than typical individual olivine grains in the AOI. Spinel is rimmed by anorthite that is itself mantled by diopside. The anorthite layers range from ~0.9 to 2.7 $\mu$m in thickness; the thickness of the outer diopside rims range from ~0.4 to 6 $\mu$m. The anorthite and diopside assemblages are about 5–60 $\mu$m in size, similar in texture to those in non-spinel-bearing AOIs.

The Lancé AOI is an elongated, 39 × 173 $\mu$m sized, spinel-bearing object (Fig. 4c) containing many voids (15.5 vol%) and cracks. Most of the olivine in the inclusion is ferroan with the low-FeO olivine concentrated mainly in the left part of the inclusion. In this portion of the AOI there is a rounded 47 × 52 $\mu$m object that superficially resembles a type-I porphyritic olivine chondrule. It consists of a dark low-FeO olivine core surrounded by anorthite.

Spinel–anorthite–diopside assemblages occur in the center of this inclusion (Fig. 4d). The spinel is mantled by anorthite

that is itself rimmed by diopside. There is a larger concentration of anorthite and diopside toward the right part of the AOI where spinel is absent. There are small (~4 $\mu$m size) grains of a Ca-P phase (probably merrillite).

The spinel in AOIs tends to increase in FeO content with increasing petrologic subtype (Fig. 5). Russell *et al.* (1998) found a similar trend in the spinel grains within CO3 refractory inclusions and attributed it to thermal metamorphism. If parent-body alteration processes are responsible for the FeO increases in the olivine of AOIs and type-I chondrules, it is plausible that these processes are also responsible for the FeO increases in spinel.

### Using Amoeboid Olivine Inclusion Observations to Refine the CO3 Chondrite Subtype Classification

Several investigators have devised classification schemes for the CO3 chondrites. McSween (1977a) assigned six CO3 chondrites to three metamorphic grades on the basis of bulk olivine and pyroxene compositions in chondrules. The Scott and Jones (1990) subtype classification is based on the FeO content and igneous zoning in chondrule olivines and pyroxenes in 11 CO3 chondrites. The Keck and Sears (1987) subtype classification is based on peak TL temperatures of whole-rock samples of nine CO3 chondrites. Kojima *et al.* (1995) based their classification on FeO in chondrule olivines in three Antarctic CO3 chondrites. Table 3 summarizes these classification schemes and presents the petrologic subtypes we recommend.

The CO3 subtypes recommended here range from 3.0 (least equilibrated) to 3.8 (most equilibrated). The changes we propose (Table 4) are based mainly on observations that AOI textures and mineral compositions reflect the substitution of $Fe^{2+}$ for $Mg^{2+}$ during whole-rock alteration more precisely than do other CO3 chondrite properties. The scheme is also based on the chondrule data of Scott and Jones (1990) and the S x-ray maps of Grossman and Rubin (1999) and J. N. Grossman (2000, pers. comm.). These maps show abundant S in the matrix of the least-altered CO3 chondrites (Y-81020 and ALHA77307) and appreciably less S in the matrix of more-altered CO3 chondrites (subtype >3.2).

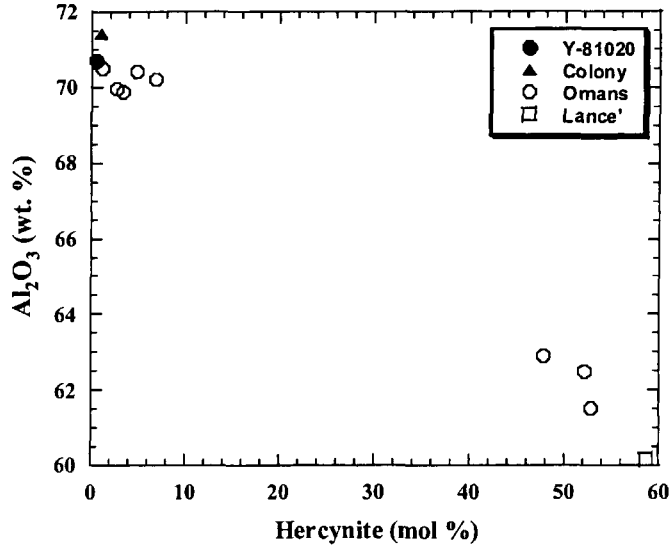


FIG. 5. AOI spinel compositions plotted as wt% $Al_2O_3$ *vs.* mol% hercynite ($FeAl_2O_4$) in four CO3 chondrites. The hercynite component of the spinel is represented by the ratio FeO/(FeO + MgO). With increasing alteration/metamorphism, FeO/(FeO + MgO) increases as $Al_2O_3$ decreases. This compositional trend is similar to that of FeO/(FeO + MgO) *vs.* $SiO_2$ in olivine. The cluster near $Hc_{50}$ may be an alteration phase rather than an altered nebular product.

We increased Kainsaz's subtype from 3.1 to 3.2 because numerous ferroan olivine veins are present, in contrast to the complete absence of such veins in the AOIs from CO3.0 chondrites. We assigned Rainbow to the same 3.2 subtype on the basis of the abundance and thickness of the ferroan olivine veins in its AOI. Bulk S distributions are similar in Rainbow

TABLE 3. Classification of CO3 chondrites by present and previous investigators.

| Meteorite | Recommended | McSween (1977a) | Scott and Jones (1990) | Sears *et al.* (1991b) | Kojima *et al.* (1995) |
|---|---|---|---|---|---|
| Yamato-81020 | 3.0 | – | – | – | 3.0 |
| Allan Hills A77307 | 3.0 | – | 3.0 | 3.3 | – |
| Colony | 3.0 | – | 3.0 | 3.2 | – |
| Kainsaz | 3.2 | I | 3.1 | 3.5 | – |
| Yamato-82050 | 3.2 | – | – | – | 3.1 |
| Rainbow | 3.2 | – | – | – | – |
| Felix | 3.3 | II | 3.2 | 3.4 | – |
| Ornans | 3.4 | II | 3.3 | 3.5 | – |
| Lancé | 3.5 | II | 3.4 | 3.5 | – |
| Allan Hills A77003 | 3.6 | – | 3.5 | 3.6 | – |
| Warrenton | 3.7 | III | 3.6 | 3.6 | – |
| Isna | 3.8 | III | 3.7 | 3.7 | – |

TABLE 4. The AOI characteristics used to refine the CO3 petrographic subtypes.

| Petrographic subtype | Thicknesses of ferroan olivine veins ($\mu$m) | Thicknesses of diffusive haloes ($\mu$m) |
|---|---|---|
| 3.0 | n/a | n/a |
| 3.1 | <2 | n/a |
| 3.2 | ~2.5 | n/a |
| 3.3 | ~4 | ~0.5 |
| 3.4 | ~6 | ~0.6 |
| 3.5 | 10–15 | ~0.8 |
| 3.6 | 20–30 | 2–3 |
| 3.7 | n/a | 5–8 |
| 3.8 | n/a | n/a |

Abbreviations: n/a = not applicable.

and Kainsaz (J. N. Grossman, unpubl. data). We infer that CO3.1 chondrites would show incipient vein formation (*i.e.*, ferroan olivine veins would be present but appreciably lower in abundance and thickness than those in Kainsaz, Y-82050 and Rainbow). There are currently no known members of subtype 3.1. We reclassified Y-82050 as subtype 3.2 rather than 3.1 as originally proposed by Kojima *et al.* (1995). This change is indicated by the olivine compositional distribution of AOIs in Y-82050 (Fig. 6): some grains with $Fa_{0-1}$ compositions that are common in subtype 3.0 are still found in subtype 3.2, similar to those found in Kainsaz and Rainbow. Furthermore, subtypes 3.3–3.8 have a peak at $Fa_{60-75}$ which is absent in Y-82050.

We recommend that the subtypes of all the other CO3 chondrites in this study be increased by 0.1 to reflect the full spectrum of their alteration. For example, what was previously classified 3.2 (Felix) should now be 3.3 because it shows systematically more advanced alteration than that shown by Kainsaz, Y-82050 and Rainbow. This trend should continue into the higher subtypes so that Warrenton and Isna would now be 3.7 and 3.8, respectively. We argue that these changes make our classification scheme less arbitrary than previous schemes because the new classifications of Warrenton and Isna are consistent with the uniform olivine compositions in these meteorites, which are similar in their uniformity to those of type 3.7–3.8 ordinary chondrites (*e.g.*, Sears *et al.*, 1991a,b). We try to quantify the differences among CO3 subtypes in the following section.

Although we have no peak-temperature or duration-of-heating data to corroborate the CO3 reclassification, our proposed refinement produces a classification scheme that differs only slightly from those of Scott and Jones (1990) and Kojima *et al.* (1995). Their classifications are based on Mg/Fe ratios in type-I and type-II chondrules which have typical grain sizes of 5–100 $\mu$m, and are thus much coarser grained than AOIs. The chondrules are therefore less sensitive to alteration than the smaller grains in AOIs.

## Variation of Amoeboid Olivine Inclusions with Increasing Petrologic Subtype

Figure 7 shows BSE images of AOIs of different subtypes. Olivine in AOIs from CO3.0 chondrites (Y-81020, ALHA77307, Colony) is forsteritic ($Fa_{0-3}$); virtually no ferroan olivine is present (Fig. 7a,b). At petrologic subtype 3.2 (Kainsaz, Rainbow, Y-82050), forsteritic olivine is rimmed by abundant ~0.25 $\mu$m thick veins of ferroan olivine (Fig. 7c). The ferroan olivine tends to conform to the shape of the outlines of pre-existing cracks and grain boundaries. The ferroan olivine veins thicken systematically as the subtype increases (Fig. 7d–f) until subtype 3.7 (Warrenton, Fig. 7g) is reached. Here, the low-FeO olivine has been entirely replaced by ferroan olivine in all but the single largest AOI observed in this study (524 × 1029 $\mu$m). In CO3.8 Isna, the most altered CO3 chondrite (Fig. 7h), the olivine is entirely ferroan ($Fa_{64-67}$).

As the ferroan olivine veins thicken and replace the low-FeO olivine in subtypes 3.2–3.7, the boundaries between the low-FeO olivine and the ferroan olivine become more poorly defined. At about subtype 3.3, diffusion halos develop around the relic low-FeO cores (Fig. 7d). With increasing subtype, the FeO gradients become shallower (Fig. 7d–f). These halos separate the low-FeO olivine cores from the ferroan olivine veins, particularly in CO3.5 Lancé and CO3.6 ALHA77003 (Fig. 7e,f). The halos are ~0.5 $\mu$m thick in Felix (subtype 3.3), ~0.8 $\mu$m thick in Lancé (3.5) and ~5 to 8 $\mu$m thick in Warrenton (3.7). It appears that the low-FeO olivine cores themselves become richer in FeO with increasing petrologic subtype, typically from $Fa_{<1}$ in type 3.0 to $Fa_{\sim 10}$ in type 3.6 (Fig. 6).

Although we analyzed the apparent centers of olivine grains with the electron microprobe, because of uncertainties in the location of grain boundaries and the location of grain centers relative to the plane of the section, many of the analyses are not of actual grain centers. Nevertheless, these data reveal systematic changes in olivine composition with petrologic subtype (Fig. 6). In Y-81020 and ALHA77307 essentially all the olivine compositions plot in low-FeO peaks (0–3 mol% Fa). About 20% of the olivine analyses in Colony are in the $Fa_{12-15}$ range; because many olivine grains in Colony AOIs contain several volume-percent limonite veins, we suggest that these ferroan olivine compositions reflect contamination by iron oxides during the severe terrestrial weathering of this meteorite (Rubin *et al.*, 1985). In Kainsaz and Rainbow, the low-FeO olivine peaks are between 5 and 10 mol% Fa, indicating that even these subtype 3.2 rocks have experienced appreciable alteration. Felix (subtype 3.3), Ornans (3.4) and Lancé (3.5) show bimodal olivine compositional distributions representing low-FeO olivine cores (3 to 10 mol% Fa) and ferroan olivine veins and rims (58 to 75 mol% Fa).

The olivine compositional distributions for Kainsaz, Rainbow and Y-82050 (Fig. 6) show intermediate Fa values between 10 and 45 mol% Fa. Because of the small size of the veins (~0.25 $\mu$m) relative to the electron beam (1–3 $\mu$m), these

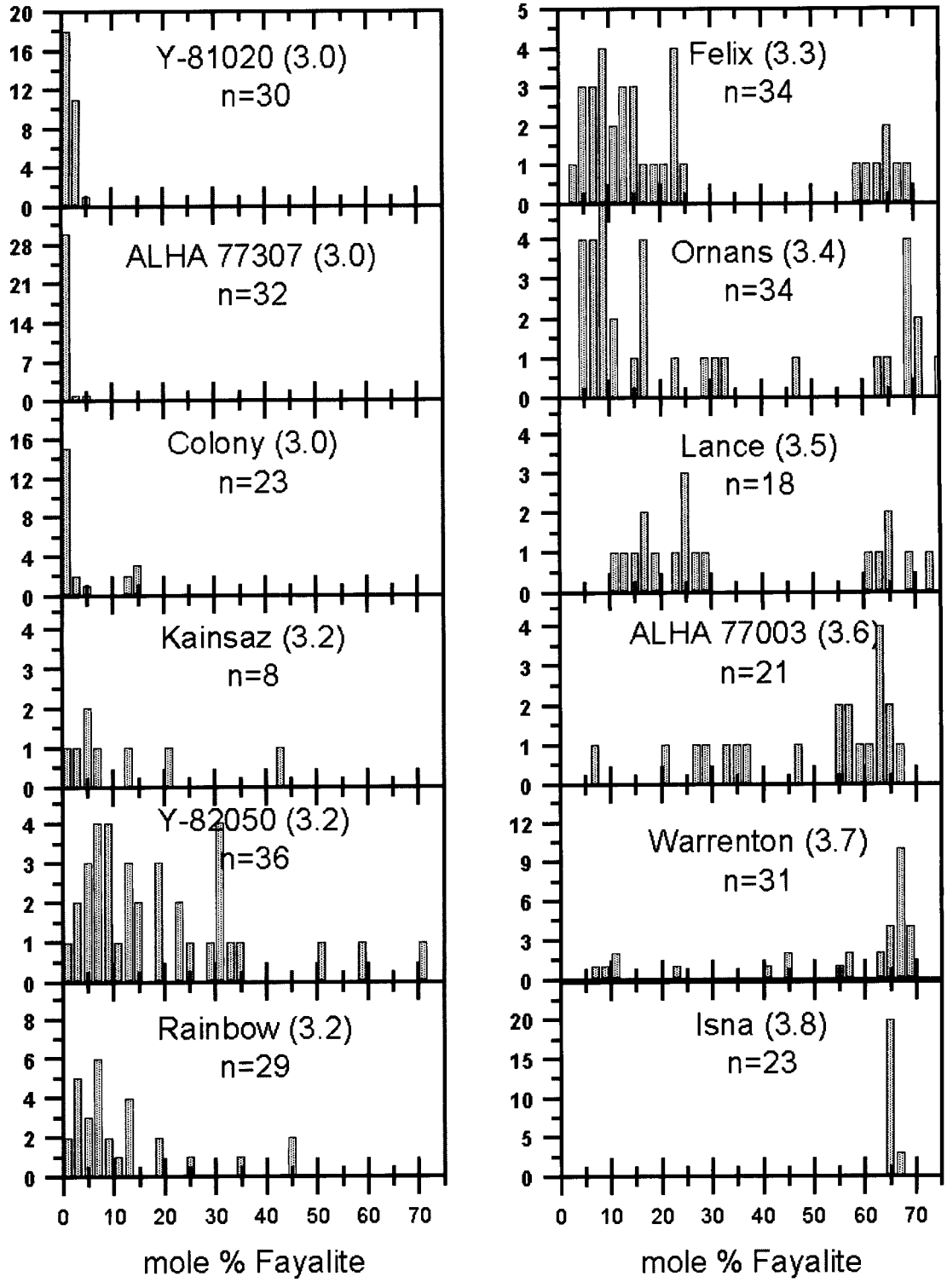


FIG. 6. Compositional distributions of olivine (in mol% Fa) in AOIs in CO3 chondrites. The petrologic sequence begins with all of the olivine occurring as forsterite (as in the CO3.0 chondrites Y-81020, ALHA77307 and Colony). The olivine grains in Colony with compositions of $Fa_{10-15}$ were probably oxidized due to terrestrial weathering. The subtype 3.2 chondrites have a broad olivine compositional distribution that peaks at $Fa_{3-10}$. As the petrologic type increases, a secondary peak develops at $Fa_{60-70}$ and no forsteritic olivine remains. At subtype 3.6, the only peak is at $Fa_{60-70}$, but a long low-Fa tail remains. At subtype 3.8 (Isna) only a narrow peak of ferroan olivine at $Fa_{\sim 65}$ occurs.

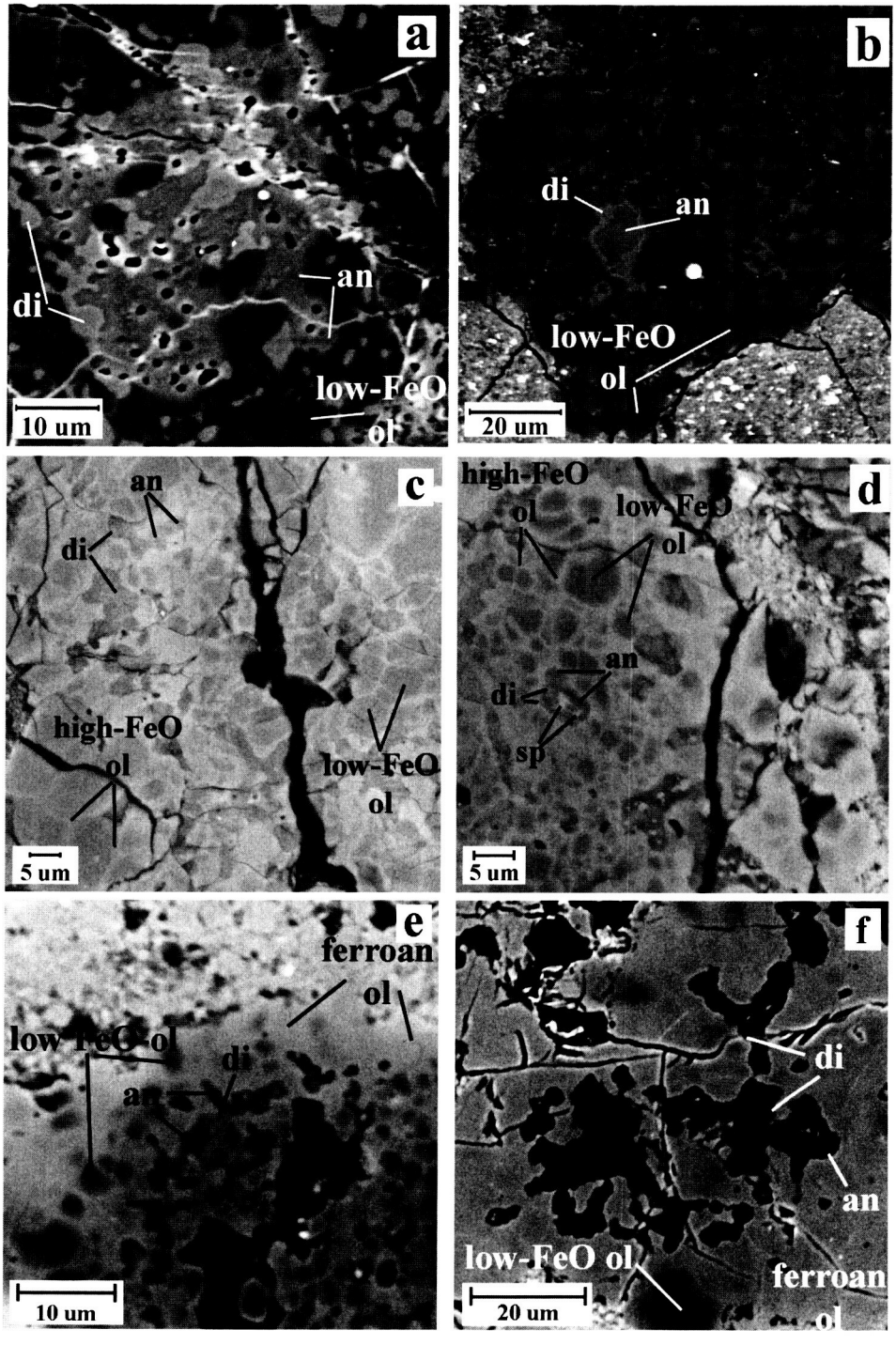


FIG. 7. Backscattered electron images of AOIs demonstrating the systematic textural changes that occur with increasing degrees of alteration. (a) CO3.0 Y-81020. (b) CO3.0 ALHA77307. (c) CO3.2 Kainsaz. (d) CO3.3 Felix. (e) CO3.5 Lancé. (f) CO3.6 ALHA77003. The CO3.0 AOI (a,b) consist of forsteritic olivine surrounding grains of diopside and anorthite; no veins of ferroan olivine are present. Note the numerous rounded pores. The CO3.2 AOI (c) consists mainly of forsteritic olivine grains surrounded by veins of ferroan olivine. The ferroan olivine veins broaden with increasing petrologic subtype (*e.g.*, 3.3–3.5) (d,e). Only rare cores of low-FeO olivine remain in subtype 3.6 (f).
*Figure 7 is continued on the following page.*

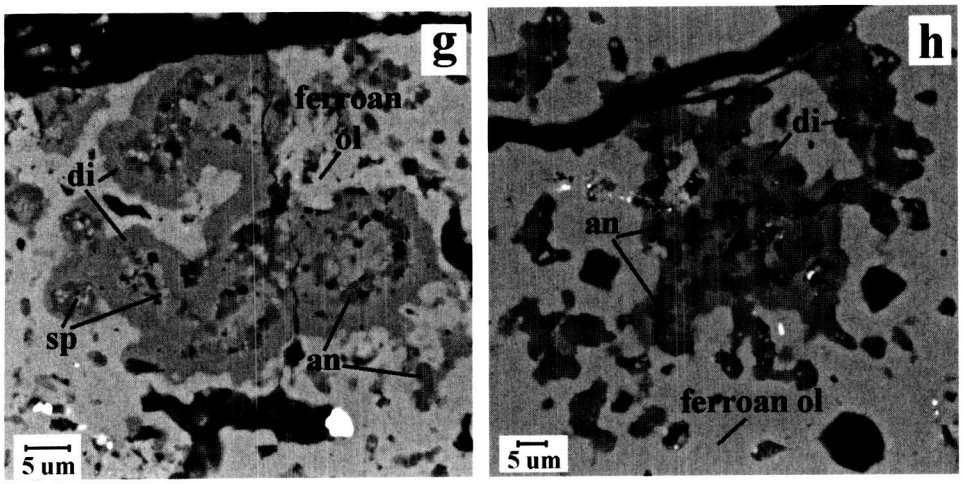


FIG. 7. *Continued.* Backscattered electron images of AOIs demonstrating the systematic textural changes that occur with increasing degrees of alteration. (g) CO3.7 Warrenton. (h) CO3.8 Isna. Low-FeO olivine is essentially absent in higher subtypes (g,h); AOIs in the CO3.7–3.8 chondrites consist of ferroan olivine surrounding grains of diopside and anorthite. Far fewer pores are visible.

TABLE 5. Selected electron microprobe analyses (wt%) of low-FeO olivine grains in AOIs.

| Meteorite | Inclusion and analysis number | $SiO_2$ | MgO | FeO | MnO | $Cr_2O_3$ | CaO | $TiO_2$ | Total | Fa (mol%) |
|---|---|---|---|---|---|---|---|---|---|---|
| Yamato-81020 | 2-64 | 42.5 | 55.5 | 0.13 | 0.09 | 0.26 | 0.08 | <0.04 | 98.6 | 0.42 |
| | 2-65 | 42.7 | 56.1 | 0.27 | 0.06 | 0.19 | 0.10 | 0.07 | 99.5 | 0.85 |
| | 5-164 | 42.7 | 56.5 | 0.23 | 0.07 | 0.26 | 0.11 | 0.08 | 100.0 | 0.72 |
| Allan Hills A77307 | 3-65 | 43.1 | 57.6 | 0.21 | 0.06 | <0.04 | 0.35 | <0.04 | 101.3 | 0.65 |
| | 4-12 | 43.9 | 57.3 | 0.19 | 0.08 | 0.06 | 0.40 | <0.04 | 101.9 | 0.59 |
| | 4-14 | 43.2 | 57.0 | 0.12 | 0.05 | <0.04 | 0.79 | 0.04 | 101.2 | 0.37 |
| Colony | 2-132 | 42.2 | 56.1 | 0.44 | 0.12 | 0.11 | 0.19 | <0.04 | 99.2 | 1.4 |
| | 2-139 | 42.9 | 58.3 | 0.30 | <0.04 | 0.10 | 0.19 | <0.04 | 101.8 | 0.91 |
| | 3-71 | 43.3 | 56.6 | 0.40 | 0.15 | 0.17 | 0.23 | <0.04 | 100.9 | 1.2 |
| Kainsaz | 3-54 | 42.3 | 55.6 | 1.1 | 0.05 | 0.14 | 0.06 | 0.11 | 99.4 | 3.4 |
| | 5-96 | 42.2 | 54.9 | 1.6 | 0.04 | <0.04 | 0.32 | 0.04 | 99.1 | 4.9 |
| | 5-103 | 43.0 | 56.8 | 0.63 | <0.04 | <0.04 | 0.32 | 0.04 | 100.8 | 1.9 |
| Felix | 2-32 | 42.3 | 55.0 | 1.9 | 0.19 | 0.06 | 0.21 | <0.04 | 99.7 | 5.8 |
| | 3-68 | 43.2 | 57.2 | 1.2 | 0.12 | 0.05 | 0.09 | <0.04 | 101.9 | 3.6 |
| | 4-80 | 43.1 | 56.0 | 2.0 | 0.14 | <0.04 | 0.11 | <0.04 | 101.4 | 6.0 |
| Ornans | 3-78 | 42.9 | 56.5 | 1.5 | 0.26 | 0.07 | <0.04 | <0.04 | 101.2 | 4.5 |
| | 5-92 | 43.8 | 56.6 | 2.0 | 0.25 | 0.12 | <0.04 | <0.04 | 102.8 | 5.9 |
| | 5-95 | 43.6 | 56.6 | 1.8 | 0.10 | <0.04 | 0.10 | <0.04 | 102.2 | 5.4 |

$Na_2O$, $Al_2O_3$ and $K_2O$ are below the detection limit of ~0.04 wt%.

intermediate Fa values are analytical artifacts caused by the electron beam overlapping differing proportions of low-FeO and ferroan olivine. This conclusion is consistent with the observation that the low-FeO olivine grains show no obvious diffusive boundaries in the BSE images. The same argument applies to the Fa values between 10 and 55 vol% for Felix, Ornans, Lancé and ALHA77307 (Fig. 6). The intermediate values in Warrenton are all from the same inclusion and appear to reflect diffusive equilibration. Tables 5 and 6 show selected analyses of olivine chosen to indicate the likely compositions of non-overlapping grains.

In summary, as the petrologic subtype increases, the systematic changes in AOI textures can be used along with changes in the olivine compositional distributions in AOIs to refine the classification of CO3 chondrite subtypes:

(1) In subtype 3.0 all of the olivine occurs in clusters of small forsterite grains free of FeO-rich olivine.

TABLE 6. Selected electron microprobe analyses (wt%) of ferroan olivine grains in AOIs.

| Meteorite | Inclusion and analysis number | $SiO_2$ | MgO | FeO | MnO | $Cr_2O_3$ | CaO | $TiO_2$ | Total | Fa (mol%) |
|---|---|---|---|---|---|---|---|---|---|---|
| Felix | 1-11 | 36.9 | 28.8 | 34.6 | 0.28 | <0.04 | 0.10 | <0.04 | 100.7 | 68.2 |
| | 1-13 | 36.1 | 30.5 | 31.6 | 0.24 | 0.06 | 0.11 | <0.04 | 98.6 | 64.9 |
| | 3-63 | 36.8 | 31.1 | 29.9 | 0.25 | 0.08 | 0.11 | 0.05 | 98.3 | 63.2 |
| Ornans | 2-35 | 36.0 | 26.7 | 38.3 | 0.19 | <0.04 | 0.18 | <0.04 | 101.4 | 71.9 |
| | 3-70 | 35.4 | 27.4 | 35.9 | 0.29 | 0.16 | 0.11 | <0.04 | 99.3 | 70.0 |
| | 3-72 | 35.0 | 24.3 | 38.9 | 0.30 | 0.12 | 0.12 | <0.04 | 98.7 | 74.1 |
| Lancé | 1-6 | 36.6 | 30.9 | 30.8 | 0.29 | 0.07 | 0.08 | <0.04 | 98.7 | 64.0 |
| | 13-26 | 36.1 | 27.0 | 35.3 | 0.16 | 0.05 | 0.11 | 0.07 | 98.8 | 70.0 |
| | 13-27 | 35.2 | 25.0 | 36.9 | 0.33 | <0.04 | 0.11 | <0.04 | 97.5 | 72.5 |
| Allan Hills A77003 | 5-33 | 38.7 | 35.0 | 26.9 | 0.34 | 0.10 | 0.05 | <0.04 | 101.1 | 57.8 |
| | 8-73 | 38.2 | 31.2 | 32.2 | 0.34 | <0.04 | 0.06 | 0.04 | 102.0 | 64.8 |
| | 3-96 | 38.0 | 32.1 | 30.8 | 0.26 | 0.10 | 0.09 | <0.04 | 101.4 | 63.1 |
| Warrenton | 1-9 | 36.7 | 29.9 | 34.3 | 0.28 | 0.05 | 0.05 | 0.05 | 101.3 | 67.2 |
| | 1-22 | 36.5 | 30.0 | 34.5 | 0.37 | 0.07 | <0.04 | <0.04 | 101.4 | 67.2 |
| | 5-97 | 36.6 | 28.7 | 35.2 | 0.30 | 0.05 | <0.04 | <0.04 | 100.9 | 68.6 |
| Isna | 3-64 | 36.1 | 30.3 | 32.6 | 0.29 | <0.04 | <0.04 | <0.04 | 99.3 | 65.7 |
| | 4-49 | 35.8 | 30.1 | 32.3 | 0.26 | 0.04 | 0.06 | <0.04 | 98.6 | 65.7 |
| | 5-17 | 36.4 | 30.6 | 33.0 | 0.33 | <0.04 | 0.05 | <0.04 | 100.4 | 65.8 |

$Na_2O$, $Al_2O_3$ and $K_2O$ are below the detection limit of ~0.04 wt%.

(2) In the as-yet-unrepresented subtype 3.1 there would be incipient development of narrow veins (<0.25 $\mu$m) of FeO-rich olivine (~3 to 5 mol% Fa) at forsterite grain boundaries.

(3) In subtypes 3.2–3.3 the original forsterite grains are surrounded by abundant ferroan olivine veins, ranging in thickness from 0.25 to 6 $\mu$m, that form on all surfaces including narrow cracks within grains. In subtype 3.2, the olivine compositional distributions retain some regions having $Fa_{0-1}$ compositions but there is no secondary peak at $Fa_{60-75}$; by subtype 3.3 the $Fa_{0-1}$ olivines have largely disappeared, at least at the resolution of the ~2 $\mu$m diameter beam of the electron microprobe.

(4) At subtype 3.4, thick zones of ferroan olivine, ~6 $\mu$m in thickness, have developed at the outside AOI margin.

(5) In subtypes 3.5–3.7 thick zones of ferroan olivine have formed in the AOI interior. In subtype 3.5, our olivine data show a small mode at $Fa_{10-30}$, probably due to overlap of the electron beam on low-FeO and high-FeO olivine; in subtype 3.6, there is no significant mode at low Fa contents.

(6) In subtype 3.7, there is a rather broad olivine compositional distribution between $Fa_{63-70}$. Low-FeO olivine only remains in the largest of the inclusions studied.

(7) At subtype 3.8, no low-FeO olivine remains and the high-Fa peak is narrow, $Fa_{64-67}$.

## DISCUSSION

### Possible Models of Amoeboid Olivine Inclusion Alteration

A remarkable compositional change from $Fa_1$ to $Fa_{65}$ occurred in AOI olivine during the processes that transformed primitive material resembling CO3.0 Y-81020 to moderately altered/metamorphosed CO3.8 Isna. If the amount of olivine were constant, 65% of the Mg must have been replaced by Fe. Because the amount of metallic Fe-Ni metal in CO3 chondrite whole rocks decreases with increasing subtype (McSween, 1977a), it seems likely that a major source of the Fe were these metallic Fe-Ni grains in the matrix.

The alteration events (aqueous and thermal) experienced by CO3 chondrites resulted in a wide variety of effects including the production of phyllosilicates (Kerridge, 1964; Christophe Michel-Lévy, 1969; Kurat, 1975; Ikeda, 1983; Keller and Buseck, 1990; Brearley, 1993), textural recrystallization (McSween, 1977a), mafic-mineral equilibration (McSween, 1977a) and the conversion of primary melilite in refractory inclusions into Ca-pyroxene, andradite and nepheline (Kojima *et al.*, 1995; Rubin, 1998; Russell *et al.*, 1998; Itoh *et al.*, 2000).

There are two end-member scenarios that must be examined to understand the progressive alteration of AOI through the CO3.0 to CO3.8 sequence: thermal diffusion and aqueous alteration, particularly dissolution and precipitation, similar to the model proposed for CV chondrites by Krot *et al.*, 1998a.

If thermal diffusion were the sole alteration mechanism, the ferroan olivine veinlets cutting though forsteritic cores would result from $Fe^{2+}$ diffusing from the FeO-rich matrix to the surfaces of AOI olivine, and then undergoing exchange with $Mg^{2+}$ from the olivine. Grain boundary diffusion is much faster than volume diffusion, especially in olivine (Chakraborty, 1997). The $Mg^{2+}$ would diffuse along grain boundaries and preexisting cracks to the matrix. Diffusion would cause compositional gradients to develop within the olivine grains

forming patterns similar to that of the error function (Hua and Buseck, 1998). Continued diffusion would cause the gradients to become wider (eventually reaching grain centers) and shallower from the edge to the center.

In the aqueous-alteration end-member model, FeO derived from the oxidation of metal in the matrix is transported along grain boundaries and through cracks, combined with $SiO_2$ (probably from unstable matrix phases), and deposited as fayalite in voids and cracks on or near the surfaces of AOI olivine grains. Evidence for systematic oxidation of CO3 metal comes from the decrease in metal content of CO3 whole rocks with increasing petrologic subtype (McSween, 1977a).

This discussion suggests that detailed examination of the cores of AOI olivine grains should allow us to distinguish between the aqueous alteration and thermal diffusion models. Aqueous alteration should produce a compositionally homogeneous overgrowth of ferroan olivine around unaltered forsteritic ($Fa_{\sim 1}$) cores. Thermal diffusion should produce compositional gradients around forsterite grains that gradually decrease in slope and increase in thickness with petrologic subtype.

CO3 chondrites of intermediate petrologic subtype are the key to distinguishing between these two end-member alteration processes. If thermal diffusion were the dominant alteration mechanism in all subtypes, the olivine in AOIs in type 3.3–3.6 chondrites should show continuous compositional gradients connecting low-FeO cores and more-ferroan mantles. If aqueous alteration were dominant, these AOI olivines should consist of forsterite cores sharply bounded by discrete layers of ferroan olivine. This latter case appears to reflect the actual texture, but better, high-magnification SEM images of individual AOIs in these rocks are needed to confirm the detailed textures.

Our observations suggest that some combination of these processes is responsible for the observed variations in the properties of the entire suite of CO3 AOIs. It seems that the first step in the alteration of AOIs was the filling of cracks and cavities by fayalite or FeO-rich olivine, and that no volume diffusion was required to complete this initial stage. Both FeO and $SiO_2$ entered the AOIs from the matrix. During the following stage, the metamorphic temperatures were high enough to allow appreciable volume diffusion as evidenced by the diffusive haloes observed around low-FeO olivine cores in the middle to high subtypes ($\geq$3.3). This diffusion continued to increase FeO contents of the cores until, at subtype 3.8 (Isna), the olivine in the AOI is essentially homogeneous. During this period, some Mg also diffused into and Fe out of the matrix, consistent with the tendency for CO3 chondrites of high subtype to have matrices with relatively high bulk MgO/(MgO + FeO) ratios (0.46 in types 3.7–3.8 compared to 0.35–0.37 in types 3.2–3.5; Table 1 of McSween and Richardson, 1977).

We observe fayalite contents as high as $Fa_{72}$ in Y-82050, Ornans and Lancé (Fig. 6). We suggest that these are lower limits caused by electron-beam overlap between fine-grained olivines with higher and lower fayalite values. We interpret the lower olivine Fa values in Isna AOIs ($Fa_{65}$) relative to those of lower subtypes (*e.g.*, Y-82050, Ornans, Lancé) to reflect the beginnings of equilibration of AOI olivine with olivine within porphyritic olivine chondrules that have much lower Fa contents, $Fa_{\sim 39}$ (Fig. 2 of Methot *et al.*, 1975).

Our interpretation is that, in the higher petrologic subtypes, volume diffusion produced the increasingly thick ferroan mantles around forsteritic cores within AOIs in Ornans, Lancé and ALHA77003 (Fig. 7). We infer that thermal diffusion was required to produce the uniform ferroan olivine in the AOIs in Warrenton and Isna (Fig. 6); these olivine grains are uniform in composition at the level of the ~2 $\mu$m diameter beam of the electron microprobe.

## Formation of FeO-Rich Olivine by Parent-Body Aqueous Alteration

There is substantial petrographic evidence that many occurrences of fayalitic olivine in chondrites formed by parent-body aqueous alteration. It occurs in the fine-grained matrices of the oxidized CV3 chondrites Kaba and Mokoia. These matrices also contain low-Ca phyllosilicates (saponite and Na phlogopite; Krot *et al.*, 1998a), phases that almost certainly formed by aqueous alteration. Fayalitic olivine in Kaba and Mokoia coexists with hedenbergite (Krot *et al.*, 1998a,b), an assemblage that is thermodynamically stable at the low temperatures expected from aqueous alteration (Krot *et al.*, 2000). The secondary character of fayalite–hedenbergite assemblages is evident by their replacement of magnetite-sulfide blebs within type I chondrules and by the occurrence of late-stage fayalite–hedenbergite veins that cut across fine-grained chondrule rims (Krot *et al.*, 1998a,b).

Figure 3 shows that the variability in the MnO, CaO and $Cr_2O_3$ contents of AOI olivine decreases with increasing petrologic subtype. This suggests that Mn, Ca and Cr were mobilized during whole-rock aqueous alteration and/or thermal metamorphism and have approached equilibrium concentrations in the olivine, diopside and spinel (both inside and outside the AOI); CaO partitions among olivine, diopside and anorthite. As shown in Tables 5 and 6, ferroan olivine on average contains higher amounts of MnO and lower amounts of CaO and $Cr_2O_3$ than low-FeO olivine. This is most likely due to MnO from the matrix following FeO into the newly formed olivine, and CaO and $Cr_2O_3$ going into the matrix.

## Comparison to Amoeboid Olivine Inclusions in CV3 Chondrites: Oxygen-Isotopic Compositions

Many characteristics (shape, texture, mineral composition, alteration systematics) of the AOIs in CV3 chondrites (*e.g.*, Grossman and Steele, 1976; Kornacki and Wood, 1984; Hashimoto and Grossman, 1987; Komatsu *et al.*, 2001) are similar to those in CO3 chondrites. AOIs in CV3 chondrites are generally much larger than their counterparts in CO3

chondrites, just as the chondrules and refractory inclusions are larger. Our observations concur with those of Komatsu *et al.* (2001) in regard to the primary mineral compositions of AOIs in the CV3 chondrites, with the exception of our observation of a Ca-P phase (probably merrillite) and our lack of conclusive evidence of nepheline. Due to the similarity in the alteration systematics of AOIs from CV3 and CO3 chondrites, it is plausible that the mechanisms of alteration were similar.

Our observations indicate that fayalitic and ferroan olivine formed in asteroids rather than in the solar nebula (*e.g.*, Hua and Buseck, 1998). Parent-body aqueous alteration of CV3 chondrites has been reasonably established (Kojima and Tomeoka, 1996; Krot *et al.*, 1995, 1997, 1998a,b; Choi *et al.*, 1997). Several researchers have reported evidence indicating that the CO3 parent body also experienced aqueous alteration (Kerridge, 1972; Kojima *et al.*, 1995; Rubin, 1998; Wasson *et al.*, 2001). There is only one basic asteroidal mechanism for the formation of fayalitic olivine, that is, oxidation of metallic Fe (or possibly FeS) to FeO by an aqueous fluid (Kerridge, 1972; Krot *et al.*, 1998a,b, 2000) and combination with $SiO_2$. Because the sizes of the AOIs, as well as that of their constituent olivine grains, are smaller in the CO3 chondrites than in the CV3 chondrites, the AOIs in CO3 chondrites should be affected at earlier stages of parent-body aqueous alteration.

Imai and Yurimoto (2001) analyzed the O-isotopic compositions of forsteritic olivine grains and ferroan olivine veins in an AOI from CV3 Allende and found that $\Delta^{17}O$ in forsteritic olivine (–22‰) is similar to that in refractory inclusions whereas ferroan olivine is $^{16}O$-poor ($\Delta^{17}O = -8‰$). They concluded that ferroan olivine formed during parent-body alteration. It seems likely that on the CO3, as well as on the CV parent body, early alteration involved precipitation of ferroan olivine from fluids similar to those ($\Delta^{17}O \approx -2‰$) inferred from CV magnetite studies by Choi *et al.* (1997) and suggested by Wasson *et al.* (2001) to be responsible for the alteration of CO3 melilite.

## SUMMARY

Amoeboid olivine inclusions in CO3 chondrites are sensitive indicators of parent-body alteration because they are fine grained and have high surface-area/volume ratios. They exhibit systematic changes in texture and mineral composition with increasing degrees of whole-rock alteration. We used these changes to refine the classification of CO3 petrologic subtypes.

The initial alteration seems to have been characterized by formation of $Fe_2SiO_4$ by reaction of an aqueous fluid with Fe (or FeS) and $SiO_2$. The first alteration phases precipitated at high surface-energy sites including grain boundaries, embayments, the margins of voids, and along preexisting cracks. Aqueous alteration in CO3 chondrites is substantiated by the presence of rare phyllosilicates in the matrix. In the CO3 chondrites of higher petrologic subtypes, thermal diffusion became increasingly important. The original $Mg_2SiO_4$ and the ferroan aqueous alteration product homogenized to give uniform $Fa_{65}$ olivine.

*Acknowledgments*–We thank C. E. Manning and A. J. Brearley for comments and advice, and M. Spilde for assistance with figures. D. S. Lauretta and T. Mikouchi provided very useful reviews. This work was supported in part by NASA grants NAG5-4331 (J. T. Wasson), NAG5-10421 (J. T. Wasson), NAG5-4766 (A. E. Rubin), NAG5-6082 (C. E. Manning) and NAG3-17431 (A. J. Brearley).

*Editorial handling*: E. R. D. Scott

## REFERENCES

BREARLEY A. J. (1993) Matrix and fine-grained rims in the equilibrated CO3 chondrite, ALHA77307: Origins and evidence for diverse, primitive nebular dust components. *Geochim. Cosmochim. Acta* **57**, 1521–1550.

CHAKRABORTY S. (1997) Rates and mechanisms of Fe-Mg interdiffusion in olivine at 980–1300 °C. *J. Geophys. Res.* **102**, 12 317–12 331.

CHOI B-G., MCKEEGAN K. D., LESHIN L. A. AND WASSON J. T. (1997) Origin of magnetite in oxidized CV chondrites: *In situ* measurement of oxygen isotope compositions of Allende magnetite and olivine. *Earth Planet. Sci. Lett.* **146**, 337–349.

CHRISTOPHE MICHEL-LÉVY M. (1969) Étude minéralogique de la chondrite CIII de Lancé. In *Meteorite Research* (ed. P. Millman), pp. 492–499. D. Reidel, Dordrecht, The Netherlands.

CLAYTON R. N. (1993) Oxygen isotopes in meteorites. *Ann. Rev. Earth Planet. Sci.* **102**, 12 317–12 331.

CLAYTON R. N. AND MAYEDA T. K. (1999) Oxygen isotope studies of carbonaceous chondrites. *Geochim. Cosmochim. Acta* **63**, 2089–2104.

CLAYTON R. N., ONUMA N. AND MAYEDA T. K. (1976) A classification of meteorites based on oxygen isotopes. *Earth Planet. Lett.* **30**, 10–18.

GROSSMAN J. N. AND RUBIN A. E. (1999) The metamorphic evolution of matrix and opaque minerals in CO chondrites (abstract). *Lunar Planet. Sci.* **30**, #1639, Lunar and Planetary Institute, Houston, Texas, USA (CD-ROM).

GROSSMAN L. AND STEELE I. M. (1976) Amoeboid olivine aggregates in the Allende meteorite. *Geochim. Cosmochim. Acta* **40**, 149–155.

HASHIMOTO A. AND GROSSMAN L. (1987) Alteration of Al-rich inclusions inside amoeboid olivine aggregates in the Allende meteorite. *Geochim. Cosmochim. Acta* **51**, 1685–1704.

HIYAGON H. AND HASHIMOTO A. (1999) $^{16}O$ excesses in olivine inclusions in Yamato-86009 and Murchison chondrites and their relation to CAIs. *Science* **283**, 828–831.

HUA X. AND BUSECK P. R. (1998) Fayalitic halos around inclusions in forsterites from carbonaceous chondrites. *Geochim. Cosmochim. Acta* **62**, 1443–1458.

HUSS G. R. (1990) Ubiquitous interstellar diamond and SiC in primitive chondrites: Abundances reflect metamorphism. *Nature* **347**, 159–162.

IKEDA Y. (1983) Alteration of chondrules and matrices in the four Antarctic carbonaceous chondrites ALH-77307 (C3), Y-790123 (C2), Y-75293(C2), and Y-74662 (C2). *Proc. NIPR Symp. Antarctic Meteorites* **8**, 93–108.

IMAI H. AND YURIMOTO H. (2001) Two generations of olivine-growth in an amoeboid olivine aggregate from the Allende meteorite (abstract). *Lunar Planet. Sci.* **32**, #1580, Lunar and Planetary Institute, Houston, Texas, USA (CD-ROM).

ITOH S., KOJIMA H. AND YURIMOTO H. (2000) Petrography and oxygen isotope chemistry of calcium-aluminum rich inclusions

in CO chondrites (abstract). *Lunar Planet. Sci.* **31**, #1323, Lunar and Planetary Institute, Houston, Texas, USA (CD-ROM).

KECK B. D. AND SEARS D. W. G. (1987) Chemical and physical studies of type 3 chondrites—VIII: Thermoluminescence and metamorphism in the CO chondrites. *Geochim. Cosmochim. Acta* **51**, 3013–3021.

KELLER L. P AND BUSECK P. R. (1990) Matrix mineralogy of the Lancé CO3 carbonaceous chondrite: A transmission electron microscope study. *Geochim. Cosmochim. Acta* **54**, 1155–1163.

KERRIDGE J. F. (1964) Low-temperature minerals from the fine-grained matrix of some carbonaceous meteorites. *Ann. N.Y. Acad. Sci.* **119**, 41–53.

KERRIDGE J. F. (1972) Iron transport in chondrites: Evidence from the Warrenton meteorite. *Geochim. Cosmochim. Acta* **36**, 913–916.

KOJIMA T. AND TOMEOKA K. (1996) Indicators of aqueous alteration and thermal metamorphism on the CV parent body; microtextures of a dark inclusion from Allende. *Geochim. Cosmochim. Acta* **60**, 2651–2666.

KOJIMA T., YADA S. AND TOMEOKA K. (1995) Ca, Al-rich inclusions in three Antarctic CO3 chondrites, Yamato-81020, Yamato-82050, and Yamato-790992: Record of low-temperature alteration. *Proc. NIPR Symp. Antarctic Meteorites* **8**, 79–96.

KOMATSU M., KROT A. N., PETAEV M. I., ULYANOV A. A., KEIL K. AND MIYAMOTO M. (2001) Mineralogy and petrography of amoeboid olivine aggregates from the reduced CV3 chondrites Efremovka, Leoville and Vigarano: Products of nebular condensation, accretion and annealing. *Meteorit. Planet. Sci.* **36**, 629–641.

KORNACKI A. S. AND WOOD J. A. (1984) Petrography and classification of Ca, Al-rich and olivine-rich inclusions in the Allende CV3 chondrite. *Proc. Lunar Planet. Sci. Conf.* **14th**, B573–B587.

KROT A. N., SCOTT E. R. D. AND ZOLENSKY M. E. (1995) Mineralogical and chemical modification of components in CV3 chondrites: Nebular or asteroidal processing? *Meteoritics* **30**, 748–775.

KROT A. N., SCOTT E. R. D. AND ZOLENSKY M. E. (1997) Origin of fayalitic olivine rims and lath-shaped matrix olivine in the CV3 chondrite Allende and its dark inclusions. *Meteorit. Planet. Sci.* **32**, 31–49.

KROT A. N., PETAEV M. I., SCOTT E. R. D., CHOI B-G., ZOLENSKY M. E. AND KEIL K. (1998a) Progressive alteration in CV3 chondrites: More evidence for asteroidal alteration. *Meteorit. Planet. Sci.* **33**, 1065–1085.

KROT A. N., ZOLENSKY M. E., KEIL K., SCOTT E. R. D. AND NAKAMURA K. (1998b) Secondary Ca-Fe-rich minerals in the Bali-like and Allende-like oxidized CV3 chondrites and Allende dark inclusions. *Meteorit. Planet. Sci.* **33**, 623–645.

KROT A. N., BREARLEY A. J., PETAEV M. E., KALLEMEYN G. W., SEARS D. W. G., BENOIT P. H., HUTCHEON I. D., ZOLENSKY M. E. AND KEIL K. (2000) Evidence for low-temperature growth of fayalite and hedenbergite in MacAlpine Hills 88107, an ungrouped carbonaceous chondrite related to the CM–CO clan. *Meteorit. Planet. Sci.* **35**, 1365–1386.

KURAT G. (1975) Der köhlige chondrit Lancé: Eine petrologische Analyse der komplexen Genese eines Chondriten. *Tscher. Mineral. Petrograph. Mitt.* **22**, 38–78.

MCSWEEN H. Y. (1977a) Carbonaceous chondrites of the Ornans type: A metamorphic sequence. *Geochim. Cosmochim. Acta* **41**, 477–491.

MCSWEEN H. Y. (1977b) Chemical analyses of chondrules and inclusions in chondritic meteorites. Ph.D. thesis, Department of Geologic Sciences, Harvard University, Cambridge, Massachusetts, USA. 19 pp.

MCSWEEN H. Y. AND RICHARDSON S. M. (1977) The composition of carbonaceous chondrite matrix. *Geochim. Cosmochim. Acta* **41**, 1145–1161.

METHOT R. L., NOONAN A. F., JAROSEWICH E., DEGASPARIS A. A. AND AL-FAR D. M. (1975) Mineralogy, petrology and chemistry of the Isna (C3) meteorite. *Meteoritics* **10**, 121–131.

RUBIN A. E. (1998) Correlated petrologic and geochemical characteristics of CO3 chondrites. *Meteorit. Planet. Sci.* **33**, 385–391.

RUBIN A. E., JAMES J. A., KECK B. D., WEEKS K. S., SEARS D. W. G. AND JAROSEWICH E. (1985) The Colony meteorites and variations in the CO3 chondrite properties. *Meteoritics* **20**, 175–195.

RUSSELL S. S., HUSS G. R., FAHEY A. J., GREENWOOD R. C., HUTCHISON R. AND WASSERBURG G. J. (1998) An isotopic and petrologic study of calcium-aluminum-rich inclusions from CO3 meteorites. *Geochim. Cosmochim. Acta* **62**, 689–714.

SCOTT E. R. D. AND JONES R. H. (1990) Disentangling nebular and asteroidal features of CO3 carbonaceous chondrite meteorites. *Geochim. Cosmochim. Acta* **54**, 2485–2502.

SEARS D. W. G., BATCHELOR J. D., LU J. AND KECK B. D. (1991a) Metamorphism of CO and CO-like chondrites and comparisons with type 3 ordinary chondrites. *Proc. NIPR Symp. Antarctic Meteorites* **4**, 319–343.

SEARS D. W. G., HASAN F. A., BATCHELOR J. D. AND LU J. (1991b) Chemical and physical studies of type 3 chondrites—XI: Metamorphism, pairing and brecciation of ordinary chondrites. *Proc. Lunar Planet. Sci. Conf.* **21st**, 493–512.

WASSON J. T., YURIMOTO H. AND RUSSELL S. S. (2001) $^{16}$O-rich melilite in CO3.0 chondrites: Possible formation of common, $^{16}$O-poor melilite by aqueous alteration. *Geochim. Cosmochim. Acta* **65**, 4539–4549.